Materials Letters 124 (2014) 256–260

Contents lists available at ScienceDirect

Materials Letters

journal homepage: www.elsevier.com/locate/matlet

Single crystalline β phase Cu–Zn nanowires: Synthesis and martensitic transformation

N. Haberkorn [a,*], A.M. Condó [a], M. Sirena [a], F. Soldera [b], F.C. Lovey [a]

[a] Comisión Nacional de Energía Atómica, Centro Atómico Bariloche, S. C. de Bariloche 8400, Rio Negro, Argentina
[b] Department of Materials Science & Engineering, Saarland University, D-66123 Saarbruecken, Germany

ARTICLE INFO

Article history:
Received 4 March 2014
Accepted 17 March 2014
Available online 26 March 2014

Keywords:
Nanowires
Single crystals
Martensitic transformation

ABSTRACT

Here, we report the synthesis of single crystalline β phase Cu–Zn nanowires (diameter around 150 nm and typical length up to 10 μm) by combining electrodeposition and annealing. The obtained nanowires present temperature driven martensitic transformation similar to that found in bulk samples from B2 to 9R structure. A weak influence of the dimensionality on the martensitic transformation is observed in these nanowires. The possibility to obtain bundles of single crystalline nanowires with tunable martensitic transformation temperature and hysteresis similar to that found in bulk, seems to be a fundamental approach to the development of smart nanosystems based on shape memory alloys.

1. Introduction

Shape memory alloys (SMAs) present a martensitic transformation which can be reversibly induced either by cooling and heating (giving rise to the shape memory effect) or by applying and releasing a mechanical stress (giving rise to the super-elastic effect) [1]. The transition temperatures of SMAs during the cooling process will be addressed as follows: martensitic start (M_s), and martensitic finish (M_f). Whereas during the heating process they will be addressed as austenitic start (A_s) and austenitic finish (A_f). The martensitic transformation temperature can be set by metallurgical composition. The shape memory effect is related to the possibility of memorizing different geometries in the austenitic and in the martensitic phases after a specific thermo mechanical training. Super-elastic behavior is obtained when the martensitic transformation is induced by applying stress in the austenitic phase. During the transformation the external force remains practically constant whereas mechanical work is consumed for the transformation phase. Once a deformation of ≈8% is reached, all the available austenite is transformed into the martensite. Exceeding that value SMAs respond as an ordinary elastic material or undergoes a second martensite–martensite transformation at much higher stresses (for instance the 18R to 6R martensite). In this way, a totally mechanical reversible deformation (with more than 15% of elongation) can be obtained [2]. Shape memory and super-elastic behavior have potential technological applications in Micro-Electro-Mechanical Systems (MEMS) [3]. The wide range of materials includes Ni–Ti [4], Au–Cd [5], In–Tl [6], Cu-based alloys [7], and also magnetic materials such as Fe–Pd [8] or Ni–Mn–Ga [9]. Research about the influence of low dimensionality in SMA has been carried out by etching thin films in defined geometries [3,10], and by testing the mechanical response of nanopillars obtained by milling single crystals with Focused Ion Beam [11–13]. The performance of these systems depends critically on their microstructure and dimensionality (surface/volume ratio). The control of the microstructure is fundamental in the developing of multifunctional and smart materials, oriented to miniaturization technologies.

The study of low dimensional SMA can be extended by fabricating nanowires (NWs). Usually metallic NWs are obtained by electrodeposition [14] and chemical vapor deposition [15]. But if the material has a low melting point they can also be obtained by liquid metal injection in anodized aluminum oxide (AAO) templates [6]. One of the difficulties related to the fabrication of SMA by electrodeposition is associated with the high sensitivity of their properties to small changes in the chemical composition. Recently, we have reported the possibility to tune the M_s in Cu–Zn films by making the samples in two steps, electrodeposition and annealing [16]. A Cu–Zn film is initially obtained by electrodeposition. Then it is encapsulated in a quartz ampoule together with a Cu–Zn bulk reference and annealed at temperatures up to 1173 K. A high annealing temperature is necessary to stabilize the β Cu–Zn phase. In addition, the high Zn vapor pressure and diffusivity [17] allow fixing the Zn atomic concentration in the film with the Cu–Zn bulk reference with a precision more accurate than 0.1 at%. During the thermal annealing, the Zn vapor pressure inside the

* Corresponding author. Tel.: +54 294 444 5147; Fax: +54 294 444 5299.
E-mail address: nhaberk@cab.cnea.gov.ar (N. Haberkorn).

http://dx.doi.org/10.1016/j.matlet.2014.03.101
0167-577X/

quartz ampoule is determined by the bulk reference and the precursor Cu–Zn film copies its chemical concentration. The Cu–Zn alloy presents a martensitic transformation for Zn concentrations between 38.5 at% and 41.5 at%, with a M_s [K]=2686–64 C_{Zn} [at%] (C_{Zn} is the Zn composition) which ranges from very low temperatures up to 230 K [18,19].

In this letter, the procedure previously described is applied to obtain β phase Cu–Zn NWs by confining the electrodeposition process to a polycarbonate membrane with a nominal pore diameter of 200 nm. After annealing, single crystalline NWs (with diameter around 150 nm and typical lengths up to 10 μm) are obtained. The NWs present a temperature driven martensitic transformation similar to that found in bulk samples from B2 to 9R structure [7]. Our result is auspicious due to both, the simple fabrication process and the weak influence of the dimensionality on the transformation temperature and on the features of the transformation (extension of the transformation and hysteresis).

2. Material and methods

The wires were grown following the procedure described in Ref. [16]. The solution was prepared with commercially available chemicals (Aldrich). The composition was 0.025 mol l^{-1} $CuSO_4$+ 0.06 mol l^{-1} $ZnSO_4$+0.9 mol l^{-1} $K_4P_2O_7$ (pH=8.2). Water treated by a Millipore Milli-Q system was used. The nanowires were grown under stirring at room temperature (around 293 K). The working electrode was a commercial polycarbonate template (Millipore) with nominal pore size 200 nm with an area of 0.5 cm^2. An Au thin film was deposited by sputtering on one side of the porous membrane, to be filled in and serve as a cathode. The reference was a commercial Ag/AgCl electrode. The counter electrode was a Pt wire. The nanowires were grown at constant voltage (−1.4 V vs. Ag/AgCl electrode). An agitation system was used in order to avoid hydrogen evolution over the sample, and to obtain a homogeneous growth inside the nanopores. After growing the nanowires, the Au thin film was removed from the polycarbonate template by using sand paper in order to avoid gold interdiffusion inside the Cu–Zn nanowires during the thermal annealing. The polycarbonate template (with the Cu–Zn nanowires embedded inside) was covered with tantalum foil, and encapsulated in a quartz ampoule (0.8 cm × 5 cm) together with a Cu–40.1 at% Zn bulk reference (≈ 1 g). The ampoule was purged several times with Argon before being sealed. The sample was heated from room temperature to 1173 K at 5 K min^{-1}. The temperature was stabilized during approximately 15 min (at 1173 K) and after that the ampoule was quenched in ice water. It is important to mention that better results were obtained by annealing the wires embedded in the polycarbonate template than in other attempts where the template was previously dissolved in chloroform. The polycarbonate template is discomposed during the annealing, avoiding the chemical reaction among nanowires.

Scanning electron microscopy (SEM) images were acquired with a FEI Nova NanoSEM 230. The microstructure of the films was studied by transmission electron microscopy (TEM) with a Philips CM200UT microscope operating at 200 kV. A microtemplate was developed for the transport measurement combining optic and electronic lithography. First a gold layer is deposited over a silicon substrate. Gold contact gaps between 500 nm and 2 μm are obtained by electronic lithography. Larger gold contacts are deposited using optic lithography and lift-off techniques. The manipulation of the Cu–Zn NW was done using a focused ion beam (FIB)/scanning electron microscope (SEM) dual beam FEI Helios NanoLab 600 equipped with a micromanipulator Omniprobe 100. In the first step a single nanowire was fixed to the manipulator with Pt (in situ deposition), which was then pulled out from the bundle. The nanowire was free standing with one end attached to nanomanipulator and it was transported with the manipulator. After that, the nanowire was brought to the desired position at the silicon wafer. The free end of the NW was fixed to the wafer by depositing Pt. Then the ion beam was used to cut the linkage between the tip and the NW, and the remaining end was fixed to the wafer. The electrical contacts to the gold pattern were made by Pt deposition. During the manipulation, the imaging of the NW with ions was avoided as much as possible, in order to prevent the formation of crystalline defects. Low ion currents of 30 pA to 50 pA were used for that.

The martensitic transformation in the bulk reference was parameterized using the conventional four probe electrical configuration; whereas in the nanowire, a two probe electrical configuration was used. In the latter case, the circuit had serial resistances which include: the nanowire, the gold patterns and the two sample/gold pattern contacts. The measurements were performed in a vacuum cooling machine with a temperature rate (cool down and warm up) of 0.15 K min^{-1}. The low temperature rate ensures no thermal shift between the sample and the sensor. The current density was 100 A cm^{-2}. The resistance was obtained by applying electrical current in both directions.

3. Results and discussion

Fig. 1a shows a SEM image of the precursor electrodeposited Cu–Zn NWs embedded in the polycarbonate template partially dissolved with chloroform. The NWs look uniformly distributed, show relatively low surface roughness (see Fig. 1b), and present an almost uniform circular cross section all along the wire length. The chemical composition in the electrodeposited NWs was determined by energy dispersive spectroscopy (EDS) being around Cu–30 at% Zn. This indicates that during the annealing, the Zn concentration needs to be increased to reach a similar value to the one present in the Cu–40.1 at% Zn bulk reference. Fig. 1c shows a typical free NW after being quenched in ice water from 1173 K. The NW looks uniform and its initial cylindrical geometry changes to square-like cross section geometry after annealing. The diameter of the Cu–Zn NWs is reduced to around 150 nm as consequence of an increment in their density due to segregation of electrochemical residues.

Fig. 2a shows a dark field TEM image of the microstructure of an electrodeposited NW. The microstructure presents in most cases, nanometric grains (< 30 nm) and occasionally some larger grains with diameters of the same order as that in the NWs. The electron diffraction pattern of the wires (see Fig. 2a inset) corresponds to the α Cu–Zn phase, which is FCC, in accordance with the binary phase diagram [20]. After annealing, the NWs become single crystalline with β Cu–Zn phase (see Fig. 2b). The high Zn diffusivity produces single crystalline NWs with diameters around 150 nm and lengths above 10 μm. Fig. 2b shows a typical dark field TEM image of a single crystalline β Cu–Zn NW. According to the electron diffraction pattern (see Fig. 2b inset) of the B2 structure or ordered β phase, the axial orientation of the NW corresponds to the [1 1 0] direction. Even though superlattice reflections were not observed (due to their weakness and the thickness of the wires), the ordered structure is expected to be as in bulk samples. Although most of the annealed NWs observed by TEM were single crystalline, we have also observed bicrystal NWs, clearly identified by their electron diffraction patterns or dark field images. It is important to mention that the performance in single crystalline SMAs is higher than in polycrystalline samples. On the one hand grain boundaries reduce the super-elastic behavior. On the other, the mechanical performance of SMAs during mechanical cycles in polycrystalline samples is affected by degradation

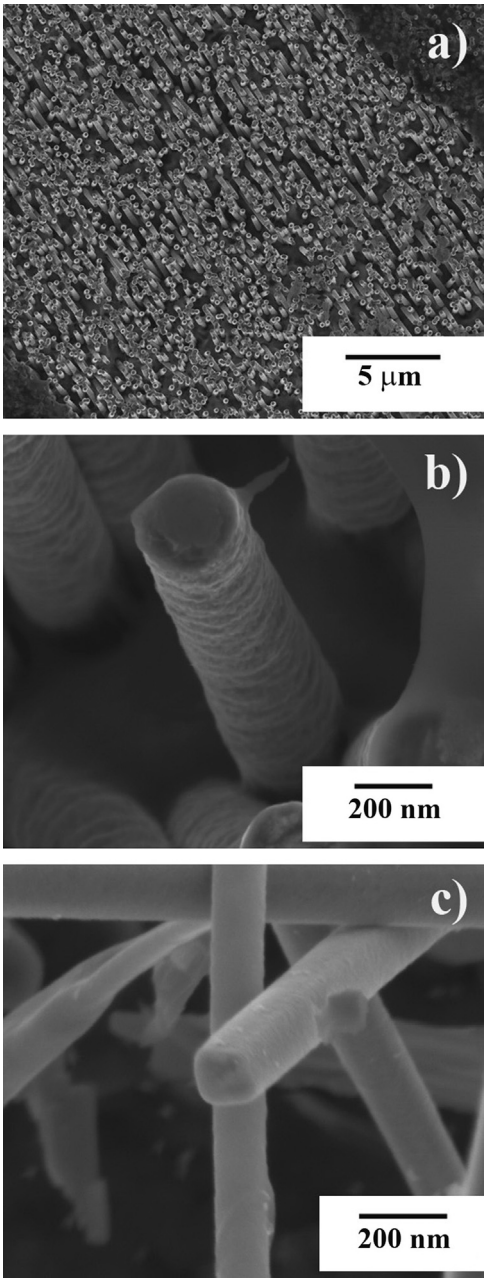

Fig. 1. SEM images of Cu–Zn nanowires. (a) Electrodeposited nanowires embedded in the polycarbonate template. (b) Single electrodeposited nanowire. (c) Annealed nanowires.

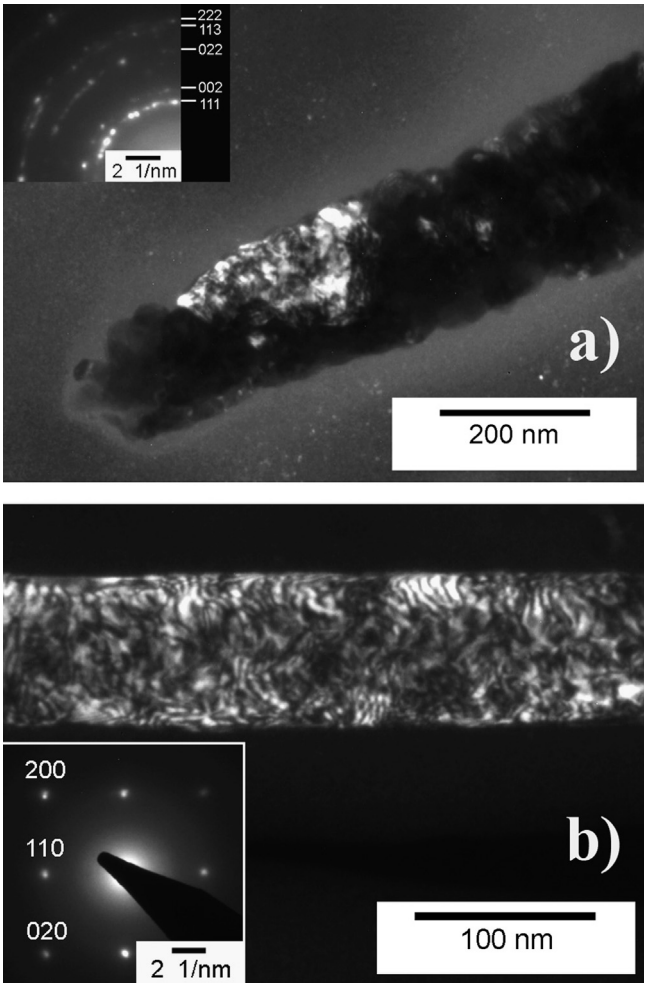

Fig. 2. (a) Dark field TEM image of an electrodeposited Cu–Zn nanowire. Inset: Corresponding α phase Cu–Zn electron diffraction rings. (b) Dark field TEM image in an annealed Cu–Zn nanowire. Inset: Corresponding [0 0 1] electron diffraction pattern of β phase. The nanowire is oriented along the [1 1 0] direction.

mechanisms such as fatigue [21]. Therefore, better mechanical and thermal driven transitions are expected in single crystalline SMAs.

Fig. 3a shows the manipulation of a β phase Cu–Zn NW using a focused ion beam (FIB)/scanning electron microscope (SEM) equipped with a micromanipulator, which is specifically placed on a nanostructured gold pattern in silicon wafer (see experimental description). The resistance was measured in a two contact configuration (see Fig. 3b). The total resistance (R) of the two-point probe configuration is expressed as $R_{2\text{point}}=R_{\text{gold}}+2R_{\text{cont}}+R_{\text{CuZn}}$. Fig. 4 shows R vs temperature (T) curves in the reference sample and a single NW (cycles number 2 and 4). The reference sample shows $M_s=126$ K and a hysteresis of 6 K. In the NW measurements, a semiconductor-like background was subtracted in order to remove electrical contact parasite resistances. The R vs. T cycles in the NW show a first order transition, with $M_s=135$ K (which is similar to the one found in the bulk and it is according to its chemical composition). It is important to mention that the hysteresis associated with the temperature driven martensitic transformation (≈ 11 K) in single crystalline NWs is within expectations for a B2→9R transformation [22], and smaller than those found in polycrystalline films (≈ 20 K) [16]. Furthermore, the extension of the martensitic transformation (M_s–M_f) in the NW is similar to that found in the bulk sample. The slight difference in the hysteresis can be related to the influence of the surface/volume ratio. In comparison with the bulk, the martensitic transformation in NWs needs larger overcooling (5–6 K), which can be related to larger driving force due to dimensional effects. This fact indicates a weak influence of the dimensionality on the temperature driven martensitic transformation with diameters above 150 nm. For example, in bulk specimens of Cu–Zn–Al the hysteresis of the β→18R ranged from 4 K to 8 K, depending on the sample condition [22]. This hysteresis is related to martensite variants nucleation and intervariant interaction. Lower hysteresis (around 0.2 K) can be obtained in a single interface transformation in a Cu–Zn–Al single crystal, were variant nucleation and intervariant interaction are avoided [23].

The low influence of the dimensionality manifested on the temperature driven martensitic transformation of β phase Cu–Zn

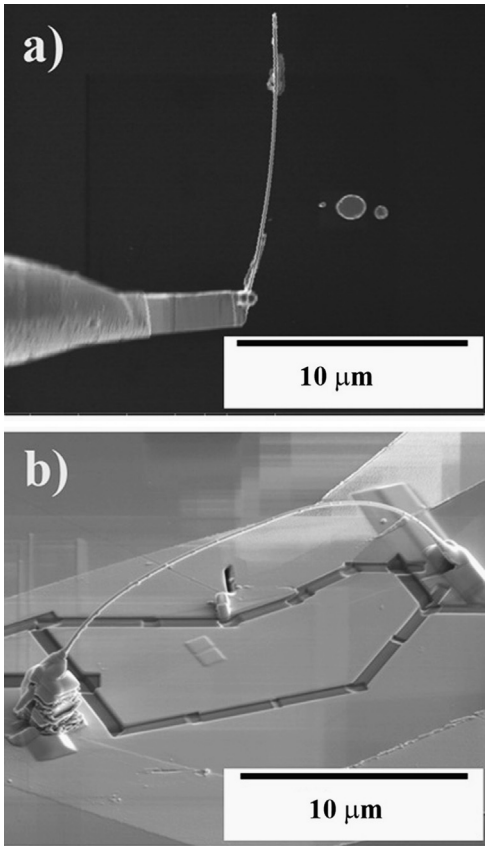

Fig. 3. (a) A nanowire is removed from the bundle, and it is brought to the desired position at the silicon wafer. The free end of the NW is fixed to the wafer by depositing Pt. (b) The nanowire is fixed to the silicon support. Electrical contacts fix the nanowire at both extremes.

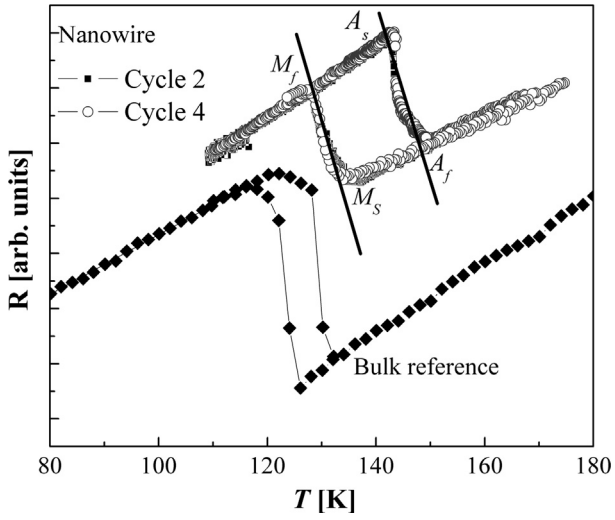

Fig. 4. Electrical transport in the Cu–Zn bulk reference and in a Cu–Zn nanowire. The thermal cycles number two and number four are included in the nanowire.

NWs should be taken into account for the development of technologies based on SMAs. On the other hand, high pseudo elastic behavior with deformation up 12% has been recently reported in Ni–Ga–Mn epitaxial thin films [24]. These results indicate that future efforts to create tiny smart machines [25] should be oriented to the synthesis of single crystalline samples.

4. Conclusions

In summary, a simple fabrication process to obtain single crystalline β phase Cu–Zn NWs is presented in this work. The results indicate low influence of the dimensionality on the B2↔9*R* martensitic transformation of Cu–Zn NWs with diameter around 150 nm. This result is in agreement with the austenitic–martensitic transformation of other nanostructured systems such as In–Tl [6]. Although mechanical tests are necessary for an overall evaluation of the performance of the Cu–Zn NWs, the fabrication of single crystalline sample bundles with tunable M_s is a fundamental first step to their possible technological applications in nanostructures or smart MEMs with functionalities at low temperatures.

Acknowledgments

We thank to C. Cotaro, E. Aburto and M. Isla for technical assistance. This work has been supported by Agencia Nacional de Promoción Científica y Tecnológica, PICT 07-02284, UN Cuyo—2011-06/C355, and CONICET PIP 2010-0457. N. H. is member of the Instituto de Nanociencia y Nanotecnología (Argentina). N. H., A. M. C. and M. S. are members of CONICET (Argentina).

References

[1] Otsuka K, Ren X. Recent developments in the research of shape memory alloys. Intermetallics 1999;7:511–28.
[2] Shuichi Miyazaki, Kazuhiro Otsuka. Development of shape memory alloys. ISIJ Int 1989;29:353–77.
[3] Wilson Stephen A, et al. New materials for micro-scale sensors and actuators: an engineering review. Mater Sci Eng, R 2007;56:1–129.
[4] Otsuka K, Ren X. Physical metallurgy of Ti–Ni-based shape memory alloys. Prog Mater Sci 2005;50:511–678.
[5] Nakanishi N, Mori T, Miura S, Murakami Y, Kachi S. Pseudoelasticity in Au–Cd thermoelastic martensite. Philos Mag 1973;28:277–92.
[6] Phillips Francis R, Dong Fang, Hongxing Zheng, Lagoudas Dimitris C. Phase transformation in free-standing SMA nanowires. Acta Mater 2011;59:1871–80.
[7] Ahlers M. Martensite and equilibrium phases in Cu–Zn and Cu–Zn–Al alloys. Prog Mater Sci 1986;30:135–86.
[8] Edler Tobias, Mayr Stefan G. Film lift-off from MgO: freestanding single crystalline Fe–Pd films suitable for magnetic shape memory actuation—and beyond. Adv Mater 2010;22:4969–72.
[9] Pons J, Chernenko VA, Santamarta R, Cesari E. Crystal structure of martensitic phases in Ni–Mn–Ga shape memory alloys. Acta Mater 2000;48:3027–38.
[10] Namazu Takahiro, Hashizume Akinobu, Inoue Shozo. Thermomechanical tensile characterization of Ti–Ni shape memory alloy films for design of MEMS actuator. Sens Actuators A 2007;139:178–86.
[11] Frick CP, Orso S, Arzt E. Loss of pseudoelasticity in nickel–titanium sub-micron compression pillars. Acta Mater 2007;55:3845–55.
[12] Ozdemir N, Karaman I, Mara NA, Chumlyakov YI, Karaca HE. Size effects in the superelastic response of $Ni_{54}Fe_{19}Ga_{27}$ shape memory alloy pillars with a two stage martensitic transformation. Acta Mater 2012;60:5670–85.
[13] San Juan J, Nó ML, Schuh CA. Superelastic cycling of Cu–Al–Ni shape memory alloy micropillars. Acta Mater 2012;60:4093–106.
[14] Xiao Feng, Hangarter Carlos, Yoo Bongyoung, Rheem Youngwoo, Lee Kyu-Hwan, Myung Nosang V. Recent progress in electrodeposition of thermoelectric thin films and nanostructures. Electrochim Acta 2008;53:8103–17.
[15] Rao CNR, Deepak FL, Gautam Gundiah, Govindaraj A. Inorganic nanowires. Prog Solid State Chem 2003;31:5–147.
[16] Haberkorn N, Ahlers M, Lovey FC. Tuning of the martensitic transformation temperature in Cu–Zn thin films by control of zinc vapor pressure during annealing. Scr Mater 2009;61:821–4.
[17] Troiani HE, Pelegrina JL, Ahlers M. The bcc-to-fcc phase transformation during dezincification of β-phase Cu–Zn. Philos Mag A 1998;78:1253–67.
[18] Ahlers M, Rapacioli R, Arneodo W The martensitic transformation in β-brass and the shape Memory effect. 1975; 379–384.
[19] Romero R, Ahlers M. On the martensitic transformation temperature and its stress dependence in Cu–Zn and Cu–Zn–Al single crystals. J Phys Condens Matter 1989;1:3191–200.
[20] Massalski T, Okamoto H, Subramanian P, Kacprzak L, editors. Binary alloys phase diagram; American Society for metals. Ohio, U.S.A: Metals Park; 1990.
[21] Melton KN, Mercier O. Fatigue of Ni–Ti thermoelastic martensites. Acta Metall 1978;27:137–44.

[22] Planes A, Macqueron JL, Rapacioli R, Guenin G. Martensitic transformation quenching effects in Cu–Zn–Al shape-memory alloys. Philos Mag A: Phys Condens Matter Struct Defects Mech Prop 1990;61:221–31.
[23] Lovey FC, Torra V. Shape memory in Cu-based alloys: phenomenological behavior at the mesoscale level and interaction of martensitic transformation with structural defects in Cu–Zn–Al. Prog Mater Sci 1999;44:189–289.
[24] Yeduru SR, Backen A, Kubel C, Wang D, Scherer T, Fahler S, Schultz L, Kohl M. Microstructure of free-standing epitaxial Ni–Mn–Ga films before and after variant reorientation. Scr Mater 2012;66:566–9.
[25] Bhattacharya Kaushik, James Richard D. The material is the machine. Science 2005;307:53–4.